sustainability

MDPI

Article

Design of Energy-Management Strategy for Solar-Powered UAV

Yuanjin Gao [1,2], Zheng Qiao [1,2], Xinbiao Pei [1], Guangxin Wu [1,2] and Yue Bai [1,*]

[1] Changchun Institute of Optics, Fine Mechanics and Physics, Chinese Academy of Sciences, Changchun 130033, China; gaoyuanjin21@mails.ucas.ac.cn (Y.G.)
[2] University of Chinese Academy of Sciences, Beijing 100049, China
* Correspondence: baiy@ciomp.ac.cn; Tel.: +86-139-9480-5899

Abstract: Energy management plays a crucial role in achieving extended endurance for solar-powered Unmanned Aerial Vehicles (UAVs). Current studies in energy management primarily focus on natural energy harvesting and task-oriented path planning. This paper aims to optimize energy consumption during the climb and glide stages by exploring variable climb speeds and glide powers. To achieve this, fitness functions are established for both the climb and glide stages, taking into account the maximum climb speed and glide power limits of the aircraft. The particle swarm optimization (PSO) algorithm is employed to solve the problem, resulting in significant energy savings of over 68% in the climb stage and 4.8% in the glide stage. Based on an analysis of the optimization trends, this study proposes an energy-management strategy to fulfill the demand for long-endurance flights. The findings of this study can serve as a valuable reference for high-altitude missions that require extended flight times.

Keywords: solar-powered UAV; high altitude long endurance; variable climb speed; variable glide power; particle swarm optimization; energy-management strategy

Citation: Gao, Y.; Qiao, Z.; Pei, X.; Wu, G.; Bai, Y. Design of Energy-Management Strategy for Solar-Powered UAV. *Sustainability* **2023**, *15*, 14972. https://doi.org/10.3390/su152014972

Academic Editor: Pablo García Triviño

Received: 29 August 2023
Revised: 26 September 2023
Accepted: 16 October 2023
Published: 17 October 2023

1. Introduction

Solar-powered UAVs are fixed-wing aircraft with a high aspect ratio that rely solely on solar energy for propulsion. The distinctive feature of solar-powered UAVs lies in their energy system, which employs solar cells to capture and convert solar radiation into usable energy during daylight hours. Excess electrical energy generated during flight is stored in batteries, allowing the aircraft to continue operating throughout the night, ensuring uninterrupted flight. Solar-powered UAV flights typically consist of four stages [1]. These stages encompass the ascent from the horizon in the morning to absorb energy, cruising at maximum altitude until insufficient light hinders flight sustainability, gliding from the maximum altitude without thrust until reaching a minimum altitude, and cruising at the minimum altitude using battery power until the next sunrise. Figure 1 depicts the various flight stages.

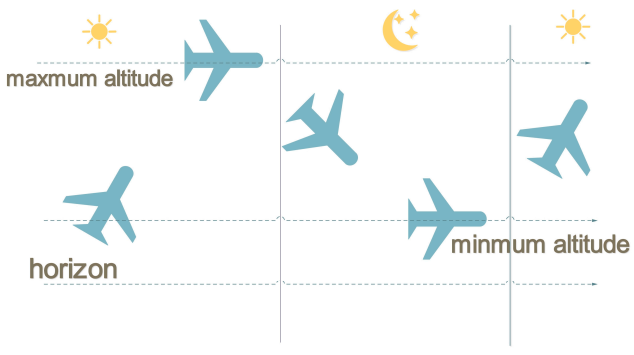

Figure 1. The four typical stages for solar-powered UAVs.

Many researchers have studied this innovative aircraft with the aim of achieving long endurance at high altitudes through the application of an energy-management system. The theoretical framework for achieving this goal involves acquiring more energy and reducing energy consumption.

1.1. Optimizing Energy Conversion

Numerous scholars have proposed novel approaches in areas such as energy acquisition and strategy transition. Mateja et al. [2] developed a mathematical model to predict solar irradiation and energy harvesting in solar-powered UAVs, incorporating various factors such as date and altitude that influence energy acquisition. They successfully validated the effectiveness of this mathematical model. He et al. proposed an energy-management system that specifically targets PV modules and storage system power under rapidly changing atmospheric conditions using a self-adaptive control strategy [3]. This system serves as the foundation for harnessing wind energy at high altitudes, specifically in the transition between the stratosphere and troposphere. Wu et al. developed dynamic models that consider factors such as wind, solar power, and temperature to meet long-endurance requirements. They proposed two energy-management system strategies, emphasizing the conversion of conditions between adjacent stages [4]. This approach has proven to be effective compared to the traditional 2-D strategy, and its research findings have a significant impact on flight projects. Avila et al. proposed a hybrid solar-battery feeding system that achieves efficient energy conversion through the implementation of sliding-mode control. Through the implementation of Maximum Power Point Tracking (MPPT), the UAV was able to maintain a constant power output, particularly for fixed-wing UAVs [5]. Currently, these researchers are improving the energy utilization efficiency and, therefore, enhancing the duration of flight through optimizing energy conversion.

1.2. Optimizing Energy by Path Planning

Moreover, extensive research has been conducted on path planning for solar-powered UAVs. Researchers have focused on optimizing the flight trajectory based on specific mission requirements, aiming to enhance energy efficiency. For instance, Wang et al. proposed a multi-objective optimization approach that combines pseudo-spectral and colony algorithms to maximize mission effectiveness and enhance the capabilities of flight missions [6]. Furthermore, a multi-objective joint strategy that includes maximum power ascent, maximum range flight, maximum glide endurance, and minimum power level flight offers more advantages compared to relying solely on solar energy utilization. Huang et al. [7] proposed a path-planning method for static targets by parameterizing state variables at each waypoint and incorporating the minimum power flight strategy. This approach simplifies the optimization process and yields optimal solutions. Another contribution by Huang et al. [8] involved the utilization of the Rapidly exploring Random Tree (RRT) algorithm for path planning. This algorithm takes into account factors such as eavesdropping, no-fly zone avoidance, and cloud coverage. By generating suitable trajectories, it ensures wireless communication without eavesdropping. Environmental influences, such as wind patterns and urban construction, have also been considered in path planning. Accurate environmental models are utilized, and researchers pay careful attention to constraints, energy models, and path-planning algorithms. Li et al. [9] employed a multi-step unscented Kalman Filter (MUKF) to predict the trajectory accurately. Furthermore, they employed a combination of the Simulated Annealing (SA) algorithm and the Quantum Particle Swarm Optimization (QPSO) algorithm to address the issues of suboptimal optimization accuracy and local minima. Using the energy model, the authors applied optimal control techniques to plan paths that optimize energy consumption under varying meteorological conditions. They also implemented a modular design for the solar-powered UAV, enabling adaptive configuration adjustments during flight. This approach introduces innovative possibilities for enhancing energy acquisition in solar-powered UAVs. However, the restriction of path

optimization to the two-dimensional plane proves to be highly limiting for high-altitude solar-powered UAVs due to the increased energy consumption during the climb stage.

1.3. Optimization in Complex Environments

Kim S. H. et al. [10] developed an energy model for solar-powered UAVs that incorporates the influence of wind fields. Building upon this, Xi et al. [11] investigated the impact of environmental conditions on the flight of high-aspect-ratio UAVs. Wind energy is considered a viable supplemental power source for flight operations. Using reinforcement learning control, energy can be extracted from the wind field to optimize navigation time. However, the availability of historical high-altitude wind field data is limited, which poses a challenge for long-term flight mission planning of solar-powered UAVs. The robust global fast terminal attractor-based control law and robust backward integral sliding-mode control (RBISMC) technique, proposed by Ullah et al. [12,13], mitigate the impact of system noise on control performance, demonstrating good convergence and tracking capabilities. These control algorithms effectively suppress noise interference and enhance the robustness and stability of the system by integrating the concepts of global fast terminal attractor and integral sliding-mode control. Additionally, the RBISMC technique achieves rapid state convergence and reduced chattering, enabling more precise trajectory tracking. These characteristics make these control algorithms highly applicable in under-actuated systems, particularly flight control in wind gradient field environments.

In summary, most research has primarily focused on increasing energy acquisition without considering the amount of energy expended during this process. Path planning has predominantly focused on the level cruise phase while neglecting significant variations in altitude and energy consumption. As a result, the climb and glide stages, which can be optimized, have been largely overlooked. The objective of this study is to examine the reduction of energy consumption during the climb and glide stages, respectively.

This paper makes the following contributions and innovations:

(1) We established fitness functions for reducing energy consumption in the climb stage and glide stage.
(2) We employed the particle swarm optimization algorithm to minimize energy loss in the process.
(3) A comprehensive analysis is conducted to analyze the energy optimization trend for longitudinal motion, resulting in the proposal of an innovative energy-management strategy. This strategy aims to guide the design of solar-powered UAVs and improve flight missions.

2. Problem Description and Modelling

Solar-powered UAVs can sustain flight during the dark night by efficiently storing solar energy during the day in batteries and gravitational potential energy. However, existing energy storage strategies often overlook energy consumption during this process, resulting in wastage. The glide stage, which occurs at the beginning of the night, requires a controlled release of gravitational potential energy to maintain flight. Traditionally, an unpowered glide is employed during this phase. However, after careful calculation, it became evident that this conventional strategy does not effectively conserve energy during the night cruise phase. Therefore, a new energy-management strategy is needed to optimize energy consumption during both the climb and glide stages.

2.1. Energy-Management Strategy Problem Description

A solar-powered UAV capable of perpetual flight would need to account for the significantly different durations of daylight during the winter solstice and summer solstice. Equipping the energy storage battery necessary for continuous flight during the winter solstice would render it inefficient and burdensome during the summer, resulting in a significant waste of payload capacity.

A solar-powered UAV in the northern hemisphere requires a 7.44 kg lithium battery to sustain flight throughout the nighttime on the summer solstice. However, during the winter solstice, when the nighttime duration increases and the gliding stage starts earlier, at least a 12.4 kg lithium battery is necessary to achieve continuous day and night flight [14]. To complete a flight mission spanning from the summer solstice to the winter solstice, a minimum of 12.4 kg lithium battery is required. The excess 4.96 kg lithium battery during the summer solstice becomes an unnecessary payload. Furthermore, at sunrise, the sunlight intensity is insufficient to meet the power requirements for a constant climb speed, leading to energy consumption from the storage battery. Therefore, optimizing energy-management strategies during the climb and glide stages is essential to reduce the number of batteries and reduce the weight of unnecessary payload.

2.2. Solar-Powered UAV Model

Many renowned solar-powered UAVs, such as Helio and Zephyr, have successfully undertaken long-endurance flight tests, reaching altitudes of up to 20,000 m [15]. However, the lack of detailed parameters for other solar-powered UAVs hinders our ability to include them in our analysis. Therefore, we have selected the Zephyr solar-powered UAV as the simulated aircraft for our study.

According to the information provided by the UK-based Zephyr project [16], we have replicated a solar-powered UAV and documented its parameters in Table 1.

Table 1. Solar-powered UAV parameter.

Name	Parameter	Number	Unit
Wing area	s	35	m^2
Weight of UAV	m	75	kg
Gravity of UAV	G	735	N
Wingspan	b	25	m
Aspect ratio	AR	17	-
Lift drag ratio	K	44	-
Zero lift coefficient	C_{L0}	0.5	-
Lift stability derivative	$C_{L\alpha}$	0.0978	-
Zero drag coefficient	C_{D0}	0.011	-
Drag stability derivative	$C_{D\alpha}$	0.0025	-

C_L and C_D represent the lift and drag coefficients, respectively, and are primarily influenced by $C_{L\alpha}$ (lift coefficient), $C_{D\alpha}$ (drag coefficient), α (angle of attack), and Ma (Mach number) [17].

$$\begin{cases} C_L = (C_{L\alpha}, \alpha, Ma) \\ C_D = (C_{D\alpha}, \alpha, Ma) \end{cases} \quad (1)$$

where α is the attack angle.

2.3. Power Consumption Model

Path planning for the solar-powered UAV can be categorized into horizontal and vertical components. The trajectory for lateral movement needs to be planned based on specific tasks, such as ground target monitoring and flight missions [18]. Due to the energy-management system controlling the longitudinal motion of solar-powered UAVs, greater emphasis is placed on vertical motion during the climb and glide stages, as compared to horizontal path planning.

The power required for level flight P_{level} and power required for climbing P_{climb} can be expressed using Equation (2) [19].

$$\begin{cases} P_{level} = \frac{GV[\rho(h)]}{K} \\ P_{climb} = G\dot{h} \end{cases} \quad (2)$$

The speed of the UAV relative to the air is represented by V, $\dot{h}$ represent the climb speed during the climb stage, G represents the gravitational force acting on the UAV.

2.4. Glide Kinematic Model

Equation (3) describes the kinematic model of a solar-powered UAV in relation to its longitudinal motion [20].

$$\begin{cases} \dot{h} = Vsin\gamma \\ \dot{V} = \frac{T-D}{m} - gsin\gamma \\ T = \frac{\rho V^2 S C_L}{2} \\ D = \frac{\rho V^2 S C_D}{2} \end{cases} \tag{3}$$

where γ represents the climb angle, while T and D denote the thrust and resistance of flight, respectively. The air density, represented by ρ, varies with the altitude of the aircraft, ranging from 20 km to 5 km, as illustrated in Figure 2.

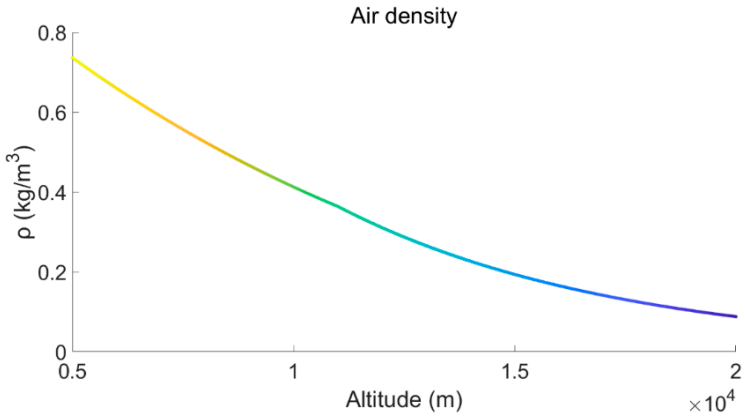

Figure 2. Air density variation according to altitude from 20 km to 5 km.

There is no thrust input when the solar-powered UAV is in the glide stage. Therefore, adjustments must be made to the kinematic model.

$$\dot{V} = -\frac{D}{m} - gsin\gamma \tag{4}$$

To streamline the calculation process, the following assumption is proposed:

Assumption 1: The aircraft operates under low attack angle and low-velocity conditions, implying a linear relationship between lift, drag, and attack angle. Based on this assumption, Equation (1) is transformed into Equation (5) [21].

$$\begin{cases} C_L = C_{L0} + C_{L\alpha} * a \\ C_D = C_{D0} + C_{D\alpha} * \alpha \end{cases} \tag{5}$$

2.5. Solar Power Model

The solar power model of a UAV is influenced by factors such as time, location, and attitude. In the context of energy-management strategies, this model can be calculated using Equation (6) [22].

$$\begin{cases} \delta = 23.45 \times \sin\left(360 \times \frac{284+dd}{365}\right),\ \delta \in [-23.45°, 23.45°] \\ \omega = 15° \times (T_{solar} - 12),\ \omega \in [-180°, 180°] \\ S_0 = \frac{12\times 3600}{\pi} \times \left[1 + 0.033 \times cos\frac{360\times dd}{365}\right] \\ S_1 = S_0 \times [\cos(\varphi)\cos(\delta)\cos(\omega) + \sin(\varphi)sin(\delta)] \end{cases} \tag{6}$$

where dd represents the number of days in a year; T_{solar} represents solar time in a day; δ represents the declination angle; ω represents the solar hour angle, which changes by 15° per hour. S_0 represents the intensity of solar radiation outside the Earth's atmosphere; S_1 represents the irradiation intensity in J/m^2; φ represents the latitude. The irradiation intensity can be calculated based on the provided date, latitude, and time.

3. Problem Conversion and Solution

Among the various metaheuristic algorithms, the particle swarm optimization algorithm stands out due to its simplicity, ease of implementation, strong global search capability, and straightforward parameter settings. PSO possesses the unique advantage of exhibiting strong parallelism, enabling particles to explore multiple solution spaces simultaneously and, therefore, accelerate the convergence of the algorithm. It is precisely this exceptional feature of PSO that makes it our preferred choice for addressing the long-endurance problem [23].

Particle swarm optimization is widely utilized in path planning and optimization tasks. Our objective is to minimize energy consumption through an efficient energy-management strategy. Therefore, we aim to optimize the traditional strategies in place. The successful implementation of PSO necessitates three main components: a fitness function, optimization variable constraints, and basic parameters such as the number of particles and iterations [24].

3.1. Fitness Function of Climb and Glide Stages

In the climb stage, the solar-powered UAV ascends from an initial altitude of h_0 at time t_0 to a final altitude of h_1 at time t_n. The energy consumed during this stage can be calculated as the integral of the sum of climb power and level power over the duration of the climb. This relationship is represented by Equation (7).

$$\int_{t_0}^{t_n} \left(G\left(\dot{h}\right) + P_{level}(h) \right) dt \tag{7}$$

In the glide stage, it is postulated that the glide commences at an altitude of h_1 and concludes at an altitude of h_0. The comparison of altitudes between powered and unpowered glides is illustrated in Figure 3. Assuming that the duration of the powered glide is denoted as t_2 and the duration of the unpowered glide is denoted as t_1. Given that the powered glide entails a longer duration, the unpowered glide attains the altitude of h_0 and transitions into the level cruise phase. To compare the two strategies, it is imperative to ensure that the time periods are equivalent. To achieve a lower energy consumption than the unpowered glide, the following conditions must be satisfied as indicated in Equation (8):

$$P_{level} \times (t_2 - t_1) > P_{glide} \times t_2 \tag{8}$$

After simplification, the expression can be represented as Equation (9):

$$\left(\frac{t_1}{t_2} + \frac{P_{glide}}{P_{level}} \right) > 1 \tag{9}$$

If Equation (9) is satisfied, we can achieve lower energy consumption compared to unpowered glide. Conversely, if Equation (9) is not satisfied, powered glide does not result in energy savings.

3.2. Constraint Condition

There are three constraints associated with the climb stage: altitude, energy, and climb speed. First, it is essential to ensure that the optimized climb speed enables the UAV to ascend to the desired altitude. Otherwise, the optimization process would be rendered meaningless. Second, in terms of energy constraint, it is crucial to guarantee that the energy acquired from solar power and energy storage batteries exceeds the energy consumed

during the climb stage. Lastly, the speed constraint dictates that the optimized climb speed must not surpass the maximum climb speed of the solar-powered UAV, therefore ensuring that the optimization results remain within the performance limits of the aircraft.

$$\begin{cases} \int_{t_0}^{t_n} \dot{h}\, dt \geq 20000 \\ \int_{t_0}^{t_n} \left(G\left(\dot{h}\right) + P_{level}(h) \right) dt < E_{bat} + \int_{t_0}^{t_n} P_{Solar}(t) dt \\ 1.5 \geq \dot{h} \geq 0 \end{cases} \tag{10}$$

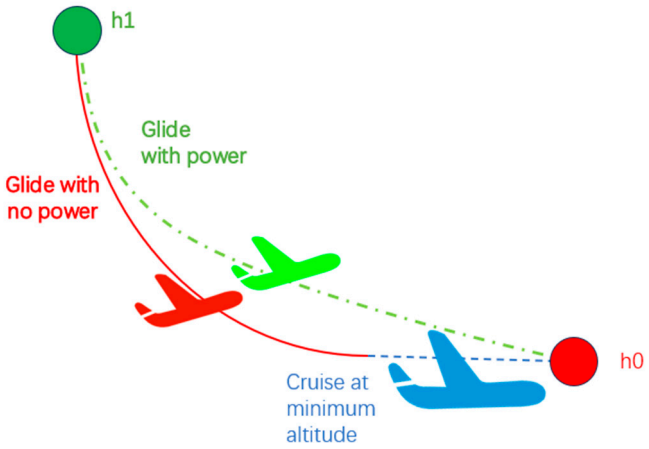

Figure 3. Schematic illustration of powered and unpowered glide at altitude.

The glide stage is subject to power limitations, as the power allocated for gliding should not surpass the upper threshold determined by optimization. In this regard, it is recommended to set the glide power to a maximum of 30 W [25].

The glide stage employs a powered glide strategy. Assuming that the number of power segments is denoted by "n". To determine the optimal number of power segments for the 20 km altitude level, the glide power remains constant. To minimize the impact of randomness in the particle swarm optimization and reduce errors caused by local optima, we adopt the average of 100 optimization results as a reference value for determining the number of power segments. As depicted in Figure 4, starting the glide at an altitude of 20 km allows for energy savings across different power segments. It is evident from the results that the optimal number of power segments is 3 when commencing the glide at 20 km.

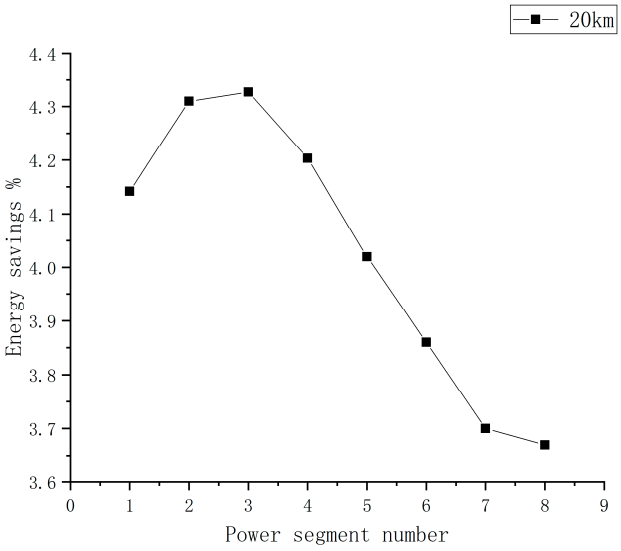

Figure 4. Relationship between the number of power segments and energy savings for power glide.

3.3. Other Parameter

The particle swarm optimization algorithm requires several essential parameters, such as the number of particles, the maximum number of iterations, and the inertia factor. To address the drawback of particle swarm optimization easily converging to local minima, we employ a strategy in which the initial particles are uniformly distributed within the solution interval. Additionally, we adaptively adjust the inertia coefficient, individual learning factor, and social learning factor to enhance the optimization process. These modified parameters can be represented as Equation (11) [26]:

$$\begin{cases} \omega = \omega_{max} - \frac{iter}{iter_{max}}(\omega_{max} - \omega_{min}) \\ c_1 = c_{max} - \frac{iter}{iter_{max}}(c_{max} - c_{min}) \\ c_2 = c_{min} + \frac{iter}{iter_{max}}(c_{max} - c_{min}) \end{cases} \tag{11}$$

where $iter$ and $iter_{max}$ represent the current and maximum number of iterations, respectively. ω_{max} and ω_{min} denote the upper and lower bounds of the inertia coefficient, respectively. Meanwhile, c_{max} and c_{min} are the extreme values associated with the learning factor. This approach serves to enhance the diversity of particles throughout the iterative process of the particle swarm optimization algorithm, facilitating rapid convergence to the optimal solution. The values of these four parameters adhere to the standard particle swarm optimization algorithm. Table 2 presents the fundamental parameter configurations for particle swarm optimization.

Table 2. The basic parameter values of particle swarm optimization algorithm.

Name	Parameter	Value
Minimum inertia coefficient	ω_{min}	1.3
Maximum inertia coefficient	ω_{max}	0.9
Learning factor minimum	c_{min}	0.2
Learning factor maximum	c_{max}	1.8
Population of particles	p	50
Maximum number of iterations	$iter_{max}$	100
Current iteration	$iter$	-

The flowchart illustrating the particle swarm optimization algorithm is depicted in Figure 5.

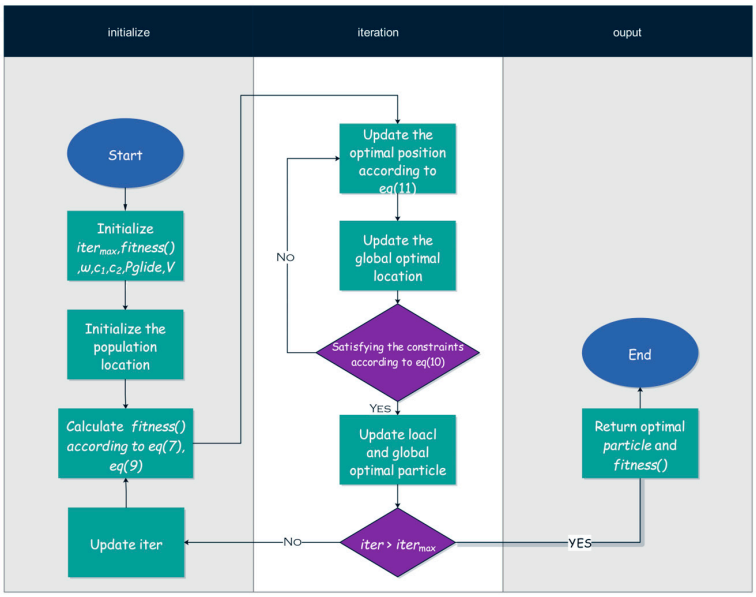

Figure 5. Flowchart of particle swarm optimization algorithm.

4. Optimize Results and Analysis

To facilitate a comparison with the traditional strategy, we evaluated the efficacy of employing a fixed climb speed of 0.8 m/s during the ascent, as well as the unpowered glide stage, under the traditional strategy. The optimization outcomes by MATLAB encompassed a comparison of altitude for the climb and glide stages, power optimization results, and an assessment of energy before and after optimization.

4.1. Simulation Results

During the climb stage, the altitude variation over time is depicted in Figure 6. Assuming both the green and red triangles represent the same time instance. It can be observed that, under the traditional strategy, the red triangle reaches an altitude exceeding 12,000 m. Conversely, the results of optimization indicate that the altitude is lower than 12,000 m. Hence, after optimization, the attained altitude is comparatively lower than the initial altitude.

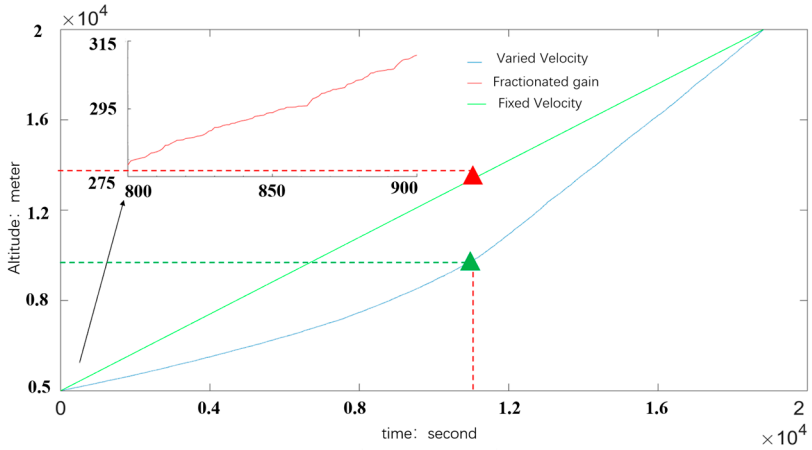

Figure 6. Altitude-time comparison before and after optimization.

For the initial generation of the climb stage, the energy consumption was calculated at a constant speed of 0.8 m/s. The iteration curve reveals a significant decline in historical minimum energy consumption within the first 100 iterations. Following seven breakthroughs in energy consumption, it eventually reached 5.12 × 10^6 J in the 44th generation, representing the minimum value achieved through this optimization process. The energy consumption, when compared to the initial iteration, was reduced by 68% (Figure 7).

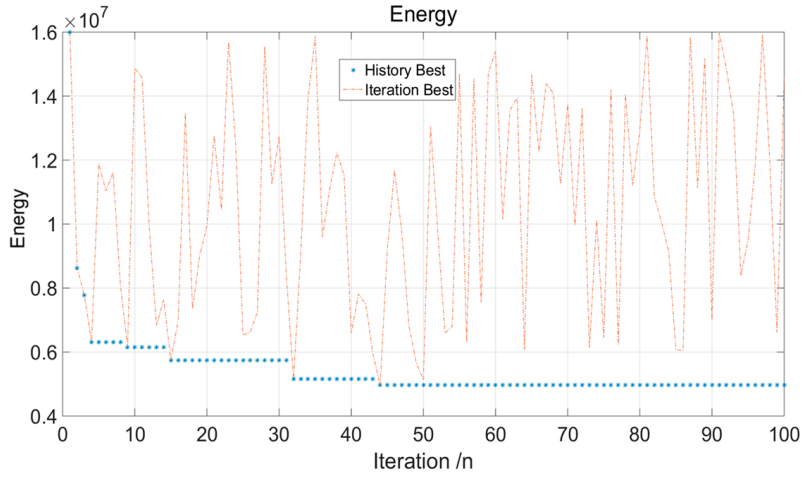

Figure 7. Minimum energy consumption change during iteration.

Due to the vulnerability of particle swarm optimization to local optimal values, even with the implementation of uniform particle distribution and parameter adaptive adjust-

ment, there is no guarantee that each optimization iteration will yield the global optimal solution. To address this, a cube is utilized to demonstrate the results of 100 particle swarm optimizations during the glide stage. Within this representation, the three coordinate axes, namely P1, P2, and P3, correspond to the power values of the three glide segments. The colors employed in the figure indicate the amount of energy savings under different power combinations (Figure 8). To visualize the optimization trend more effectively, the section of the cube that exceeds the average energy savings is displayed separately (Figure 9).

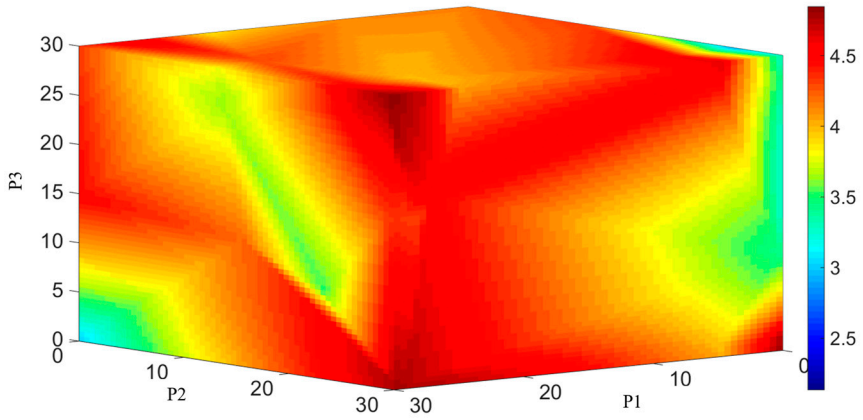

Figure 8. Energy savings from 100 optimization results.

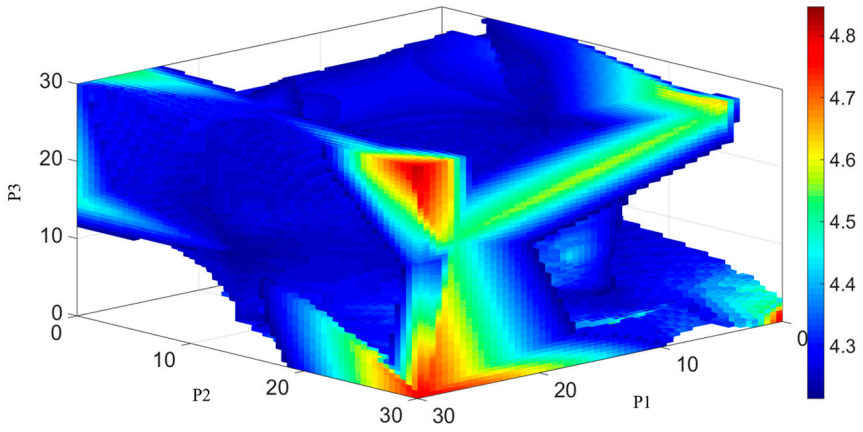

Figure 9. The above-average portion of energy savings.

The altitude profiles of a single optimization result are depicted in Figure 10, illustrating the distinct differences. Both unpowered glide and powered glide commence at an altitude of 20 km and conclude at 5 km. In this optimization result, the power values for the powered glide are 27.4, 26.5, and 28.1, respectively. Throughout the descent, the powered glide consistently maintains a lower altitude compared to the unpowered glide, with the unpowered glide ending at 25,211 s and the powered glide at 27,897 s. Ultimately, a 4.2% energy savings is achieved.

To bolster the credibility of our findings, we conducted a comparative analysis with Wang et al.'s multi-objective genetic algorithm, known as NSGA-II [27]. This multi-objective optimization involves simultaneously optimizing three energy objectives: acquired solar energy, charged energy, and consumed energy. Through comparison, it has been discovered that this approach can acquire more energy. However, it requires maintaining a certain tilt angle of the UAV, which leads to an increase in energy consumption during the energy acquisition process. Moreover, the additional energy consumed is much greater than the extra energy acquired. This is illustrated in Figure 11. In other words, the simultaneous optimization of energy acquisition and energy consumption during the climb stage in an NSGA-II framework, instead of yielding higher total energy, paradoxically results in a

decrease in overall energy. The energy of charging can be regarded as passive energy that depends on acquisition and consumption and cannot be optimized through active control. Therefore, optimizing the objective function based on the consumed energy alone yields better results in the climb stage. In the glide stage, since there is no solar energy available, there is also no charged energy and only the last energy objective remains meaningful. This aligns with the objective function of this paper.

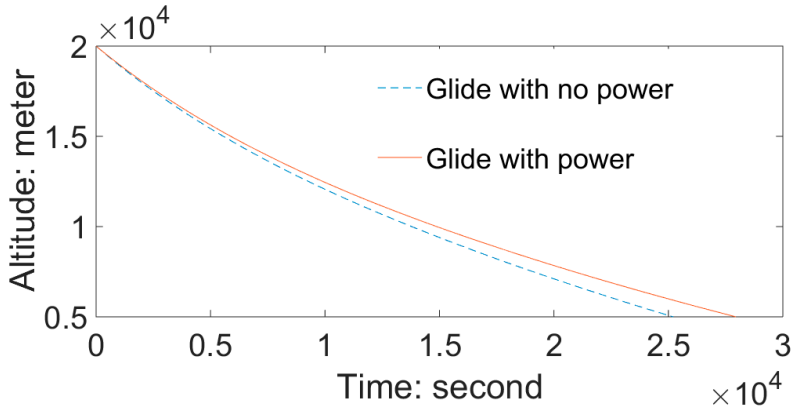

Figure 10. A comparative depiction of altitude-time profiles before and after optimization during the glide stage.

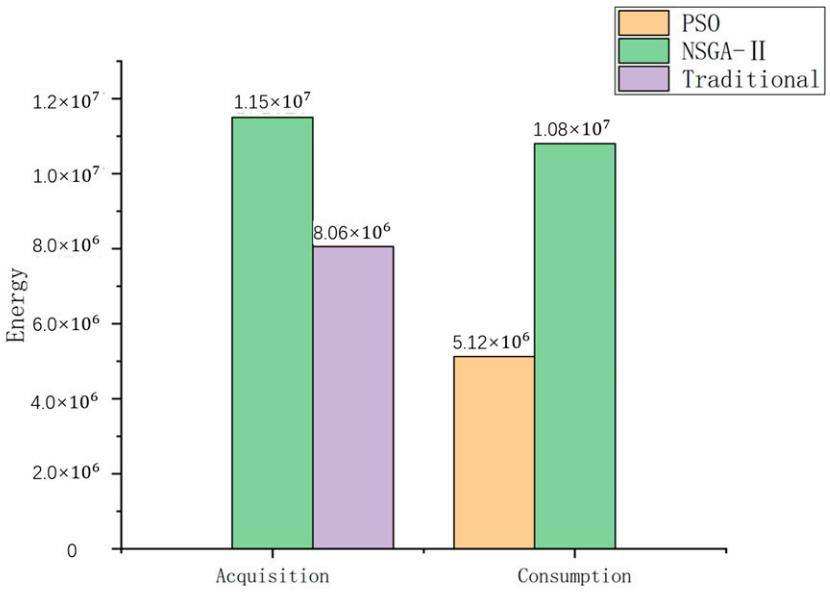

Figure 11. Comparison of energy acquisition and consumption in climb stage.

The comparison is visually depicted in Figure 12. Our particle swarm optimization algorithm outperforms the traditional strategy by achieving remarkable energy savings of 68% during the climb stage, spanning from 5 km to 20 km. Similarly, in the glide stage from 20 km to 5 km, our algorithm achieves energy savings of 4.8% compared to the traditional strategy. In contrast, the multi-objective genetic algorithm yields energy savings of 32.6% during the climb stage and 3.7% during the glide stage. These calculations provide concrete evidence that our method not only achieves superior energy savings in the glide stage but also significantly reduces energy consumption in the climb stage.

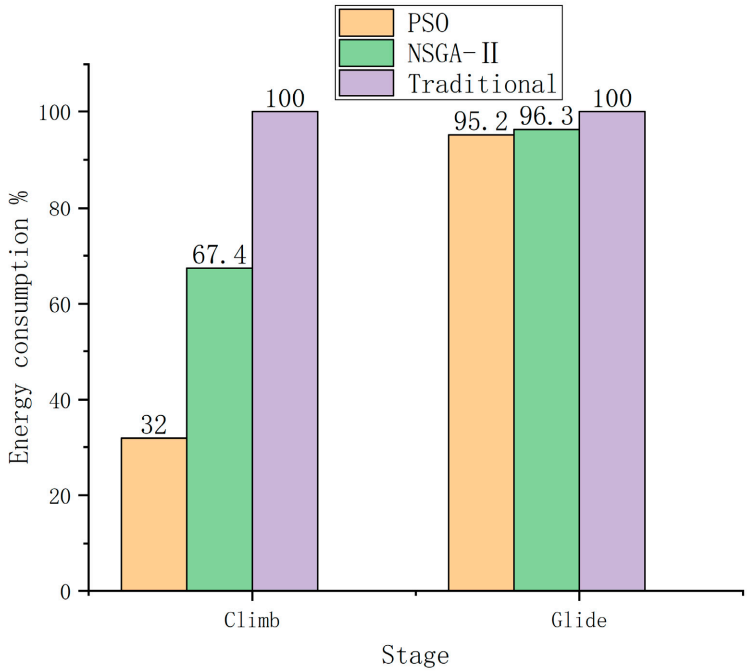

Figure 12. Comparison of energy consumption among 3 strategies.

4.2. Optimization Trend Analysis

To devise energy-management strategies suitable for long-endurance requirements, it is imperative to conduct separate analyses of the optimization trends during the climb and glide stages. This will enable mission planners and solar-powered UAV designers to enhance energy utilization efficiency. To this end, a comprehensive analysis of the fitness function, upon which particle swarm optimization is based, is necessary for understanding the optimization trend.

The fitness function for the climb stage is divided into two parts. The first part pertains to the climb power, with the integral of the climb stage representing the gravitational potential energy. However, the climb power cannot be optimized when the altitude difference remains constant, as gravitational potential energy is solely dependent on the altitude difference. The second part focuses on the level of flight power, which is influenced by air density and positively correlated with speed. As the climb altitude gradually increases, the air density decreases, requiring an increase in speed to maintain lift. This increase in speed leads to a corresponding rise in the level of flight power. From our perspective, the optimization tendency is to delay the time taken to reach a specific altitude.

The optimization trend of the glide stage can be analyzed using Equation (9). For glide missions at a specific altitude, the unpowered glide time (t_1) and the levelling power (P_{level}) for cruising at the designated altitude are determined. The only variables that need to be optimized are the glide time (t_2) and the glide power (P_{glide}). Increasing the glide power can prolong the glide time, but it also has a negative impact on the fitness function value. Conversely, increasing the glide time has a positive effect on enhancing the fitness function value. The objective of optimization is to find the solution that maximizes the function value by considering both the positive and negative effects.

The optimization results presented in Figures 8 and 9 indicate that the negative effect of increasing glide power is not as significant as the positive effect. Hence, increasing the glide power to improve the glide time maximizes the fitness function value and conserves energy.

The primary objective of optimizing the climb stage is to replace the high-power consumption associated with level flight in traditional strategies with a lower power consumption during low-altitude flight. The climb stage can be considered to be a phase dedicated to exchanging altitude for energy conservation. Similarly, the optimization of the glide stage aims to replace the power required for level flight at cruising altitude with

a maximum glide power limit of only 30 W. Through calculations, it is determined that approximately 200 W of power is necessary to maintain level flight at an altitude of 5 km. The glide stage can be seen as a stage where power is exchanged for energy conservation.

4.3. New Energy-Management Strategy

Figure 13 illustrates the altitude diagram of the particle swarm optimization algorithm before and after optimization. The red line represents the altitude change using the traditional strategy, while the green line represents the energy-saving strategy post-optimization.

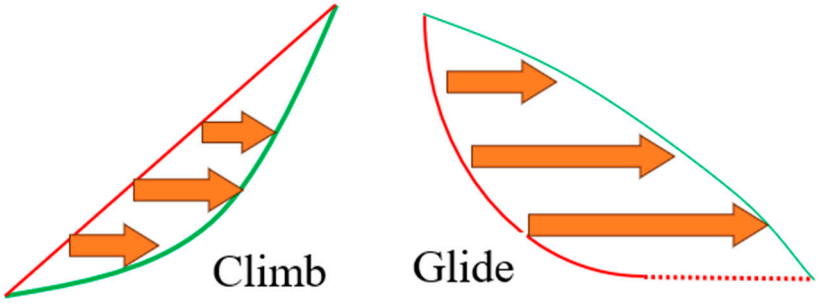

Figure 13. Schematic diagram of climb and glide stages optimization trends at altitude.

Based on the analysis of the optimization trends presented in Figure 13 and Table 3, a novel energy-management strategy is proposed. During the climb stage, it is recommended to strategically delay the ascent to a specific altitude while ensuring the capability to reach the desired target altitude. In the glide stage, extending the glide duration through an increase in glide power is advised to effectively minimize energy consumption.

Table 3. Climb and glide stage optimization trend and energy comparison.

Stage	Optimization Trend	Energy Savings
Climb	Delay time to a certain altitude	68%
Glide	Delay the glide to the lower altitude	4.8%

5. Conclusions

This paper makes two main contributions. First, it establishes an optimization model for variable climb speed and variable glide power, resulting in reduced energy consumption during the climb and glide stages. The energy savings achieved are more than 68% during the climb and 4.8% during the glide. Second, based on quantitative analysis of the optimization trend, an energy-management strategy for the climb and glide stages, with a focus on achieving long endurance, is proposed.

The energy management and path planning of solar-powered UAVs possess a unique appeal not found in other types of UAVs. It is our earnest desire to encourage increased participation of researchers in the scientific exploration of path planning and solar-powered UAVs. Each endeavor in this research domain is certain to unlock opportunities for visionary advancements, ultimately driving the prosperity of solar-powered UAV technology.

Author Contributions: Conceptualization, Y.G.; methodology, Y.G.; software, Y.G.; validation, Y.G.; formal analysis, Y.G.; resources, Y.G.; data curation, Y.G.; writing—original draft preparation, Z.Q.; writing—review and editing, Y.G.; visualization, G.W.; supervision, Z.Q.; project administration, Y.B.; funding acquisition, X.P. All authors have read and agreed to the published version of the manuscript.

Funding: This research was supported in part by the Innovation Fund of the Chinese Academy of Sciences, under grant CXYJJ20-ZD-03, and in part funded by the Regional Development Young Scholars Program of the Chinese Academy of Sciences.

Institutional Review Board Statement: Not applicable.

Informed Consent Statement: Not applicable.

Data Availability Statement: Not applicable.

Acknowledgments: The authors would like to thank Yue, Bai at Changchun Institute of Optics, Fine Mechanics and Physics (CIOMP), Chinese Academy of Sciences, for his time and technical support in this research work.

Conflicts of Interest: The authors declare no conflict of interest.

References

1. Gao, X.Z.; Hou, Z.X.; Guo, Z.; Liu, J.X.; Chen, X.Q. Energy management strategy for solar-powered high-altitude long-endurance aircraft. *Energy Convers. Manag.* **2013**, *70*, 20–30. [CrossRef]
2. Mateja, K.; Skarka, W.; Peciak, M.; Niestrój, R.; Gude, M. Energy Autonomy Simulation Model of Solar Powered UAV. *Energies* **2023**, *16*, 479. [CrossRef]
3. He, X.; Sun, X.; Wang, F.; Li, X.; Zhuo, F.; Luo, S. Design of Energy Management System for a Small Solar-Powered Unmanned Aerial Vehicle. In Proceedings of the 2018 9th IEEE International Symposium on Power Electronics for Distributed Generation Systems (PEDG), Charlotte, NC, USA, 25–28 June 2018; pp. 1–4.
4. Wu, J.; Wang, H.; Huang, Y.; Su, Z.; Zhang, M. Energy management strategy for solar-powered UAV long-endurance target tracking. *IEEE Trans. Aerosp. Electron. Syst.* **2018**, *55*, 1878–1891. [CrossRef]
5. Avila, E.; Jaramillo, A.; Costa, J.; Pozo, M.; Borja, G.; Madera, P.; Paredes, A.; Otero, N.; Condolo, V.; Vintimilla, A. Energy Management of a Solar-Battery Powered Fixed-Wing UAV. In Proceedings of the 2018 International Conference on Information Systems and Computer Science (INCISCOS), Quito, Ecuador, 13–15 November 2018; pp. 180–185.
6. Wang, X.; Yang, Y.; Wu, D.; Zhang, Z.; Ma, X. Mission-Oriented 3D path planning for high-altitude long-endurance solar-powered UAVs with optimal energy management. *IEEE Access* **2020**, *8*, 227629–227641. [CrossRef]
7. Huang, Y.; Chen, J.; Wang, H.; Su, G. A method of 3D path planning for solar-powered UAV with fixed target and solar tracking. *Aerosp. Sci. Technol.* **2019**, *92*, 831–838. [CrossRef]
8. Huang, H.; Savkin, A.V.; Ni, W. Energy-Efficient 3D navigation of a solar-powered UAV for secure communication in the presence of eavesdroppers and No-Fly zones. *Energies* **2020**, *13*, 1445. [CrossRef]
9. Li, K.; Han, Y.; Yan, X. Distributed multi-UAV cooperation for dynamic target tracking optimized by an SAQPSO algorithm. *ISA Trans.* **2022**, *129*, 230–242. [CrossRef]
10. Kim, S.H.; Padilla, G.E.G.; Kim, K.J.; Yu, K.H. Flight path planning for a solar-powered UAV in wind fields using direct collocation. *IEEE Trans. Aerosp. Electron. Syst.* **2019**, *56*, 1094–1105. [CrossRef]
11. Xi, Z.; Wu, D.; Ni, W.; Ma, X. Energy-Optimized Path planning for Solar-Powered Aircraft in a Wind Field Using Reinforcement Learning. *IEEE Access* **2022**, *10*, 87715–87732. [CrossRef]
12. Ullah, S.; Mehmood, A.; Khan, Q.; Rehman, S.; Iqbal, J. Robust Integral sliding mode control design for stability enhancement of under-actuated quadcopter. *Int. J. Control Autom. Syst.* **2020**, *18*, 1671–1678. [CrossRef]
13. Ullah, S.; Khan, Q.; Mehmood, A.; Kirmani, S.A.M.; Mechali, O. Neuro-adaptive fast integral terminal sliding mode control design with variable gain robust exact differentiator for under-actuated quadcopter UAV. *ISA Trans.* **2021**, *120*, 293–304. [CrossRef]
14. Shukla, A.; Nema, S. A Review on Strategies of Electrical Drive Utilization. In Proceedings of the Solar Powered Airplane, 2023 IEEE International Students' Conference on Electrical, Electronics and Computer Science (SCEECS), Bhopal, India, 18–19 February 2023; pp. 1–6.
15. El-Atab, N.; Mishra, R.B.; Alshanbari, R.; Hussain, M.M. Solar powered small unmanned aerial vehicles: A review. *Energy Technol.* **2021**, *9*, 2100587. [CrossRef]
16. Arum, S.C.; Grace, D.; Mitchell, P.D.; Zakaria, M.D.; Morozs, N. Energy Management of solar-powered aircraft-based high altitude platform for wireless communications. *Electronics* **2020**, *9*, 179. [CrossRef]
17. Zhang, Z.J.; Ji, R.T.; Wang, Y.; Chang, M.; Ma, X.P.; Sha, J.; Mao, D.L. An improved energy management strategy for the solar powered unmanned aerial vehicle at the extreme condition. *J. Energy Storage* **2021**, *43*, 103114. [CrossRef]
18. Thipyopas, C.; Sripawadkul, V.; Warin, N. Design and Development of a Small Solar-Powered UAV for Environmental Monitoring Application. In Proceedings of the 2019 IEEE Eurasia Conference on IOT, Communication and Engineering (ECICE), Yunlin, Taiwan, 3–6 October 2019; pp. 316–319.
19. Wenjun, N.I.; Ying, B.I.; Di, W.U.; Xiaoping, M.A. Energy-optimal path planning for solar-powered aircraft using soft actor-critic. *Chin. J. Aeronaut.* **2022**, *35*, 337–353.
20. Martin, R.A.; Gates, N.S.; Ning, A.; Hedengren, J.D. Dynamic optimization of high-altitude solar aircraft trajectories under station-keeping constraints. *J. Guid. Control Dyn.* **2019**, *42*, 538–552. [CrossRef]
21. Danjuma, S.B. Aerodynamic Design Consideration for Stability of a Lightweight Solar-Powered Aircraft. *Path Sci.* **2022**, *8*, 4010–4016. [CrossRef]
22. Dwivedi, V.S.; Kumar, P.; Ghosh, A.K.; Kamath, G. Selection of size of battery for solar powered aircraft. *IFAC-PapersOnLine* **2018**, *51*, 424–430. [CrossRef]

23. Na, Y.; Li, Y.; Chen, D.; Yao, Y.; Li, T.; Liu, H.; Wang, K. Optimal Energy Consumption Path Planning for Unmanned Aerial Vehicles Based on Improved Particle Swarm Optimization. *Sustainability* **2023**, *15*, 12101. [CrossRef]
24. Menon, S.P.; Shukla, P.K.; Sethi, P.; Alasiry, A.; Marzougui, M.; Alouane, M.T.-H.; Khan, A.A. An intelligent diabetic patient tracking system based on machine learning for E-Health applications. *Sensors* **2023**, *23*, 3004. [CrossRef]
25. Sekander, S.; Tabassum, H.; Hossain, E. Statistical performance modeling of solar and wind-powered UAV communications. *IEEE Trans. Mob. Comput.* **2020**, *20*, 2686–2700. [CrossRef]
26. Lu, Z.; Wang, J.; Lian, X.; Zhang, J.; Zhang, Y.; Yang, J. Continuous Low-Thrust Maneuver Planning for Space Gravitational Wave Formation Reconfiguration Based on Improved Particle Swarm Optimization Algorithm. *Sensors* **2023**, *23*, 3154. [CrossRef] [PubMed]
27. Wang, H.; Li, P.; Xiao, H.; Zhou, X.; Lei, R. Intelligent energy management for solar-powered unmanned aerial vehicle using multi-objective genetic algorithm. *Energy Convers. Manag.* **2023**, *280*, 116805. [CrossRef]